Conformational Changes of Yeast Plasma Membrane H^+-ATPase during Activation by Glucose: Role of Threonine-912 in the Carboxy-Terminal Tail†

Silvia Lecchi, Kenneth E. Allen, Juan Pablo Pardo,‡ A. Brett Mason, and Carolyn W. Slayman*

Departments of Genetics and Cellular and Molecular Physiology, Yale University School of Medicine, New Haven, Connecticut 06510

Received August 4, 2005; Revised Manuscript Received October 14, 2005

ABSTRACT: Yeast Pma1 H^+-ATPase, which belongs to the P-type family of cation-transporting ATPases, is activated up to 10-fold by growth on glucose, and indirect evidence has linked the activation to Ser/Thr phosphorylation within the C-terminal tail. We have now used limited trypsinolysis to map glucose-induced conformational changes throughout the 100 kDa ATPase. In the wild-type enzyme, trypsin cleaves first at Lys-28 and Arg-73 in the extended N-terminal segment (sites T1 and T2); subsequent cleavages occur at Arg-271 between the A domain and M3 (site T3) and at Lys-749 or Lys-754 in the M6−M7 cytoplasmic loop (site T4). Activation by glucose leads to a striking increase in trypsin sensitivity. At the C-terminal end of the protein, the Arg- and Lys-rich tail is shielded from trypsin in membranes from glucose-starved cells (GS) but becomes accessible in membranes from glucose-metabolizing cells (GM). In the presence of orthovanadate, Lys-174 at the boundary between M2 and the A domain also becomes open to cleavage in GM but not GS samples (site T5). Significantly, this global conformational change can be suppressed by mutations at Thr-912, a consensus phosphorylation site near the C-terminus. Substitution by Ala at position 912 leads to a GS-like (trypsin-resistant) state, while substitution by Asp leads to a GM-like (trypsin-sensitive) state. Thus, the present results help to dissect the intramolecular movements that result in glucose activation.

Over the past two decades, Pma1 H^+-ATPase of yeast and other fungi has become a well-studied prototype for the large, widely distributed family of cation-transporting P-type ATPases (*1*, *2*). The H^+-ATPase is the single most abundant protein in the yeast plasma membrane and has been estimated to split more than 20% of cellular ATP. It pumps protons out of the cell electrogenically, creating the primary ion gradient that drives the H^+-coupled uptake of nutrients and helping to maintain a proper cytoplasmic pH.

Not surprisingly, multiple mechanisms have evolved to regulate the amount and activity of the H^+-ATPase in the plasma membrane (*3*). Prominent among them is a rapid, posttranslational activation by glucose, first observed by Serrano in 1983 (*4*) and confirmed since then in other laboratories (*5*−*7*). In a typical experiment, the addition of glucose to carbon-starved cells leads within minutes to a 5−10-fold increase in ATPase activity, accompanied by a lowering of the K_m for MgATP and IC_{50} for vanadate and an alkaline shift in pH optimum. Growing evidence links the kinetic changes to a release from autoinhibition by the carboxy-terminal tail of the 100 kDa ATPase, brought about by kinase-mediated phosphorylation of one or more Ser/Thr residues. Consistent with this idea, Portillo, Serrano, and co-workers (*8*, *9*) have reported that site-directed mutagenesis at consensus phosphorylation sites within the carboxy-terminal region can suppress the glucose effect, and Mason and co-workers (*10*) have found that deletion of the last 18 residues leads to constitutive activation. Furthermore, upon digestion of the ATPase with thermolysin, Chang and Slayman (*11*) observed the rapid appearance of two new phosphopeptide fragments following the addition of glucose; an important goal of future research will be to identify these phosphorylation sites directly.

In the meantime, recent work has begun to shed light on later steps of the activation process. During a site-directed mutagenesis study of the H^+-ATPase, Miranda and co-workers observed that Cys substitutions along one face of stalk segment 5, an α-helical extension of membrane segment 5 (M5) into the cytoplasmically located P domain (*12*, *13*), led to a constitutive stimulation of ATPase activity in the absence of glucose (*14*). The same mutant enzymes also displayed kinetic parameters that are normally characteristic of the activated state. A follow-up study, using a membrane-impermeant fluorescent maleimide as a probe, showed that cysteines at three positions on the opposite face of S5 are hidden to the aqueous medium in H^+-ATPase from glucose-starved cells but become exposed in preparations from glucose-metabolizing cells (*15*). Thus, it is clear that glucose-mediated activation proceeds by way of a significant conformational change in the central catalytic portion of the ATPase.

Given the structural complexity of the 100 kDa ATPase (*12*, *13*), the present study was undertaken to investigate the physical extent of the glucose-dependent change. Using

† This work was supported by research grant GM15761 from the National Institute of General Medical Sciences.

* Corresponding author. Tel: 203-737-1770. Fax: 203-737-1771. E-mail: carolyn.slayman@yale.edu.

‡ Present address: Departamento de Bioquimica, Facultad de Medicina, UNAM, Ap. Postal 70159 Mexico D.F., 04510 Mexico.

10.1021/bi051555f CCC: $30.25
Published on Web 11/22/2005

limited trypsinolysis in the presence and absence of physiologically important ligands such as MgADP and orthovanadate, we have examined H^+-ATPase preparations from glucose-starved and glucose-metabolizing cells. Wild-type ATPase has been compared with mutants bearing amino acid substitutions at two consensus phosphorylation sites near the carboxyl terminus of the enzyme (Ser-899 and Thr-912). The results indicate that glucose brings about a global conformational change in the H^+-ATPase. Interestingly, mutations at position 912 have the ability to suppress this change, holding the ATPase in a conformation that resembles either the "glucose-starved" state (T912A) or the "glucose-metabolizing" state (T912D).

EXPERIMENTAL PROCEDURES

Site-Directed Mutagenesis. Strain NY13 (*MAT*a ura3-52) of *Saccharomyces cerevisiae* was used in this study. Mutations were introduced at positions S899 and T912 by the polymerase chain reaction using the "megaprimer" method of site-directed mutagenesis (*16*). A 1.2 kb *Sal*I/*Sac*I restriction fragment containing the mutated sequence was subcloned into a modified Bluescript II KS(±) plasmid (Stratagene, La Jolla, CA) carrying the *PMA*1 fragment *Bam*HI/*Xba*I, and the 2.1 kb *Bam*HI/*Sac*I fragment was then moved to the yeast vector YCp2*HSE-PMA*1 containing the full-length *PMA*1 gene (*17*). To integrate the mutations into the yeast genome, the 1.3 kb *Bgl*II fragment containing each mutation was subcloned into the pGW201 vector (*18*) modified by the addition of a second *Bgl*II site downstream of the *PMA*1 coding sequence. The 6.1 kb *Hin*dIII fragment containing the mutant allele linked to *URA*3 was then excised from the plasmid and integrated into yeast strain NY13 using the alkali-cation yeast transformation kit (Bio 101). DNA sequencing of the entire gene confirmed the presence of the desired mutation.

Preparation of Plasma Membranes from Glucose-Starved and Glucose-Metabolizing Cells. As described by Serrano (*19*), cells were grown to midexponential phase at 30 °C in supplemented minimal medium containing 4% glucose, harvested, washed twice with water, and incubated with shaking for 1 h in water without glucose. Glucose (4%) was then added back to an aliquot of the culture for 30 min (glucose-metabolizing cells, GM), while another aliquot was kept in glucose-free medium (glucose-starved cells, GS). Plasma membranes were prepared from both aliquots (*20*), washed with 1 mM EGTA/Tris (pH 7.5), and resuspended in a small volume of the same buffer. All procedures were carried out at 0−4 °C. Protein concentrations were determined by the method of Lowry et al. (*21*) as modified by Ambesi et al. (*22*).

Quantitation of Expressed ATPase. To determine the level of expressed Pma1 protein, membranes were subjected to SDS−polyacrylamide gel electrophoresis and immunoblotted with affinity-purified polyclonal antiserum against the closely related Pma1 ATPase of *Neurospora crassa*. Quantitative PhosphorImager (Molecular Dynamics) analysis was carried out at two different protein concentrations within the linear range, and the expression level was calculated from the average of two or more determinations.

ATP Hydrolysis. ATP hydrolysis was assayed at 30 °C in 0.5 mL of 50 mM MES/Tris, pH 5.7, 5 mM NaN_3, 5 mM Na_2ATP (Roche), 10 mM $MgCl_2$, and an ATP-regenerating system (5 mM phosphoenolpyruvate and 50 μg/mL pyruvate kinase). The reaction was terminated after 20 min by the addition of Fiske and Subbarow reagent, and the release of inorganic phosphate from ATP was measured (*23*). Specific activity was calculated as the difference between ATP hydrolysis in the presence and absence of 100 μM sodium orthovanadate (Fisher). IC_{50} values for vanadate inhibition were determined by measuring ATP hydrolysis in the presence of increasing concentrations of vanadate from 0.1 to 100 μM. To determine the K_m for MgATP, Na_2ATP was varied between 0.2 and 6 mM, with $MgCl_2$ always in excess of ATP by 5 mM; the actual concentrations of MgATP were calculated by the method of Fabiato and Fabiato (*24*). K_m and V_{max} were determined by fitting the data with either the Michaelis−Menten or Hill equation using SigmaPlot software.

Tryptic Digestion. Plasma membranes were diluted to 1 μg/μL in buffer containing 20 mM Tris, pH 7.0, and 10 mM $MgCl_2$ in the presence or absence of ATPase ligands (10 mM MgADP or 100 μM VO_4). After incubation at 30 °C for 5 min, trypsin (Worthington) was added to the membrane samples at a trypsin:protein ratio of 1:4. Proteolysis was stopped at the desired time by the addition of diisopropyl fluorophosphate (DFP) to a final concentration of 1 mM. Samples (0.5 μg) were then subjected to electrophoresis in 4−15% SDS−polyacrylamide gels, electrotransferred to nitrocellulose, and treated with either affinity-purified antiserum against Pma1 ATPase of *N. crassa* or affinity-purified antiserum against the carboxy-terminal 18 amino acids of the yeast ATPase (*25*). Anti-rabbit antibody, HRP conjugated (Promega), was used to identify antigen−antibody complexes, and the signal was detected by ECL (Amersham Biosciences). Densitometry analysis was performed using an Umax Astra 3400 scanner and Image Quant 5.0 software (Molecular Dynamics).

Amino Acid Sequencing. Proteolytic products were separated by SDS−PAGE, electroblotted to PVDF membrane, and stained with Coomassie Blue. Amino acid sequences of specific bands cut from the PVDF membrane were determined by Edman degradation in Yale University's W. M. Keck Foundation Biotechnology Resource Laboratory.

RESULTS

Location of Tryptic Cleavage Sites in Wild-Type H^+-ATPase. The first step in this study was to ask whether limited trypsinolysis could serve as a useful tool to track glucose-dependent conformational changes in wild-type H^+-ATPase. In the experiment of Figure 1, plasma membranes from GS and GM cells were incubated at a trypsin:protein ratio of 1:4 from 0 to 20 min. Reactions were stopped by adding DFP, and digestion of the ATPase was tracked as a function of time by SDS−polyacrylamide gel electrophoresis and immunoblotting. When such a blot was probed with polyclonal antiserum against the entire 100 kDa Pma1 ATPase (Figure 1A), major bands of 98 kDa (a) and 87 kDa (b) appeared rapidly and decreased over time, while a 57 kDa band (e) was generated more gradually, reaching a maximum at 5−10 min. Less abundant bands of 75 kDa (c), 68 kDa (d), 50−45 kDa (f triplet), and 26 kDa (h) could also be detected. While there was no appreciable difference

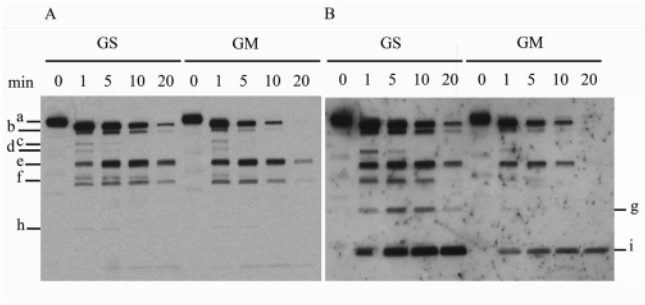

FIGURE 1: Effect of glucose activation on the time course of trypsinolysis of wild-type ATPase. Plasma membranes from glucose-starved (GS) and glucose-metabolizing (GM) cells were incubated at a trypsin:protein ratio of 1:4 for 0−20 min as described in Experimental Procedures. Aliquots (0.5 μg of protein) were then analyzed by immunoblotting with polyclonal anti-Pma1 antiserum (panel A) or antiserum against the carboxy-terminal 18 amino acids of the ATPase (panel B).

Table 1: Fragments Obtained from Limited Trypsinolysis of Yeast H^+-ATPase

band	sequence	mobility[a] (kDa)	Ab binding[b] Pma1	Ab binding[b] C-term
Pma1		100	*	*
a	^{29}TY	98	*	*
b	^{74}PVPEEYLQ	87	*	*
c		75	*	
v	^{175}TLANTAVV	73	*	
d		68	*	*
e	^{272}AAALVNKA	57	*	*
i		20		*

[a] Relative mobility calculated from SDS−PAGE. [b] Antibody binding was determined in immunoblots using affinity-purified polyclonal antiserum against the closely related Pma1 ATPase of *N. crassa* (Pma1) or affinity-purified antiserum against the carboxy-terminal 18 amino acids of the yeast ATPase (C-term). See Experimental Procedures.

in either the number or sizes of bands between GS and GM conditions, GM samples displayed a conspicuous acceleration in the *rate* of trypsinolysis, pointing to a general "opening" of ATPase structure during glucose activation.

To gain further information about the tryptic fragments seen in Figure 1A, the same blot was reprobed with antiserum against the last 18 residues of the ATPase (Figure 1B). In both GS and GM samples, the three major bands (a, b, and e**)** and at least two of the minor bands (d and f) were still visible, indicating that they contained most or all of the carboxy-terminal tail. In addition, the C-terminal antiserum detected two smaller bands, both of which were significantly more prominent in the GS sample than in the GM sample. These were band g (36 kDa) and band i (20 kDa), the latter being highly resistant to further degradation by trypsin (Figure 1B).

For the three abundant large bands (a, b, and e), the tryptic cleavage sites were readily mapped by N-terminal protein sequencing. As shown in Table 1, band a was produced by cleavage between Lys-28 and Thr-29 (T1 in Figure 2) and band b, by cleavage between Arg-73 and Pro-74 (T2 in Figure 2), both sites located in the amino-terminal region of the ATPase. Band e resulted from cleavage between Arg-271 and Ala-272 (T3 in Figure 2) toward the end of the small cytoplasmic loop between transmembrane segments 2 and 3 (M2 and M3). Although it was not possible to sequence the 20 kDa band (i), its apparent size and the presumed

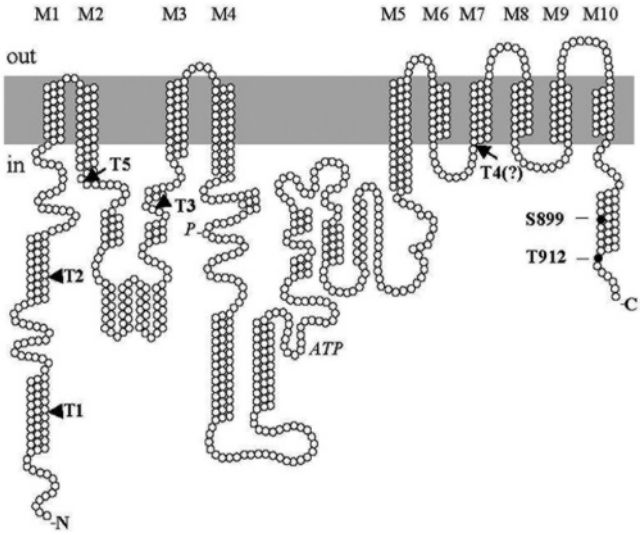

FIGURE 2: Topological diagram of yeast Pma1 H^+ATPase illustrating the location of tryptic cleavage sites T1−T5. Also highlighted are S899 and T912 in the carboxy-terminal tail, sites at which glucose-dependent phosphorylation has been proposed to activate the ATPase (*9*).

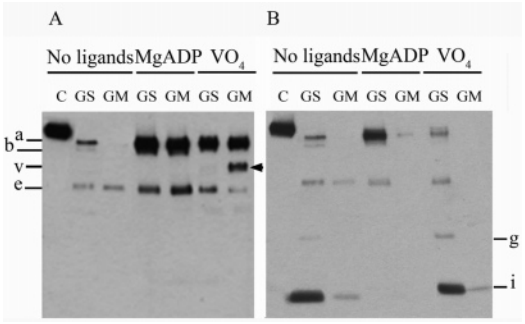

FIGURE 3: Effects of MgADP and vanadate on the trypsinolysis of wild-type ATPase. Plasma membranes from GS and GM cells were incubated for 15 min at a trypsin:protein ratio of 1:4 in the presence or absence of 10 mM MgATP or 100 μM VO_4. Aliquots (0.5 μg of protein) were then analyzed by immunoblotting with polyclonal anti-Pma1 antiserum (panel A) or anti-C-terminal antiserum (panel B). C = control (undigested) samples.

topology of the protein suggest that this cleavage occurred in the cytoplasmic loop between M6 and M7, following Lys-749 or Lys-754 (T4 in Figure 2).

Detection of Glucose-Induced Conformational Change in Wild-Type H^+-ATPase. It has long been known that proteolytic cleavage patterns of P-type ATPases can be significantly affected by physiological ligands, which have the ability to pull the protein into distinct conformational states corresponding to successive steps in the reaction cycle (*26*). For this reason, we carried out trypsinolysis in the presence of such ligands in order to gain more precise information about glucose-induced changes in the H^+-ATPase. In the experiment of Figure 3, GS and GM preparations were exposed to trypsin (1:4) for 15 min in the presence and absence of either 10 mM MgADP or 100 μM orthovanadate, which can be expected to lock the ATPase in E_1-like or E_2-like states, respectively. Immunoblotting with anti-ATPase antiserum revealed that these ligands slowed the rate of trypsinolysis significantly in both the GS and GM samples (Figure 3A).

In the case of MgADP, a striking difference between GS and GM samples became apparent upon immunoblotting with

anti-C-terminal antiserum (Figure 3B). While all three of the major tryptic fragments (bands a, b, and e) retained the C-terminus in the GS sample, all three rapidly lost it in the GM sample, providing direct evidence for the relative exposure of the carboxyl terminus under glucose-metabolizing conditions. Attempts to pinpoint the exact cleavage site have not yet been successful, but because there was no appreciable change in the mobility of a, b, and e, cleavage must have occurred at one of the numerous Arg or Lys residues very close to the carboxyl terminus (e.g., K891, K894, K896, K897, R900). The C-terminal 20 kDa fragment was no longer detectable in either the GS or GM sample in the presence of MgADP (Figure 3B).

Useful information also came from the trypsinolysis of wild-type ATPase in the presence of vanadate. Here, there was an even more pronounced difference between the GS and GM samples. When immunoblotting was carried out with anti-ATPase antiserum (Figure 3A), a new 73 kDa band (v) appeared in the GM sample but not in the GS sample and was notably resistant to further digestion by trypsin. N-Terminal Edman degradation of band v revealed that the vanadate-stimulated cleavage had occurred between Lys-174 and Thr-175 (T5), near the beginning of the cytoplasmic loop between M2 and M3 (Table 1, Figure 2); this position lies at the boundary between the P and A domains. With vanadate, as with MgADP, there was also a rapid loss of the carboxyl terminus in the GM sample, with little or no anti-C-terminal antiserum now bound by fragments a, b, e, or v (Figure 3B). The 20 kDa C-terminal fragment (i) was readily detectable in the presence of vanadate in the GS sample but barely visible in the GM sample.

Mutations at Ser-899 and Thr-912. The results up to this point provide direct experimental support for a conformational opening during activation of the H^+-ATPase by glucose, with tryptic cleavage sites becoming exposed both in the C-terminal tail and (in the presence of vanadate) at the boundary between the P and A domains. Because previous studies have implicated C-terminal Ser/Thr phosphorylation in the activation process, it was of interest to ask whether mutations of individual Ser and Thr residues in this region might alter the trypsinolysis behavior. The experiments to be described focused on two such residues: Ser-899, which lies within a consensus site for casein kinase II, and Thr-912, which forms part of a consensus site for calmodulin-dependent protein kinase II (Figure 2). On the basis of analysis by NetPhos 2.0 (*27*), these two residues have the highest phosphorylation probabilities of all serines and threonines in the carboxy-terminal tail (0.998 and 0.951, respectively), and both have been proposed to play a role in glucose regulation (*9*). Each was substituted by Ala to prevent phosphorylation and by Asp to mimic phosphorylation, and the resulting constructs were integrated into the chromosome by homologous recombination to replace the wild-type *PMA*1 gene. Three of the four mutants (S899A, S899D, T912D) grew normally on glucose-containing medium, while the fourth (T912A) grew at approximately 50% of the wild-type rate.

In the experiments summarized in Figure 4 and Table 2, plasma membranes from glucose-starved (GS) and glucose-metabolizing (GM) cells were isolated and assayed for ATPase activity over a range of MgATP and vanadate concentrations. The wild-type enzyme displayed strong

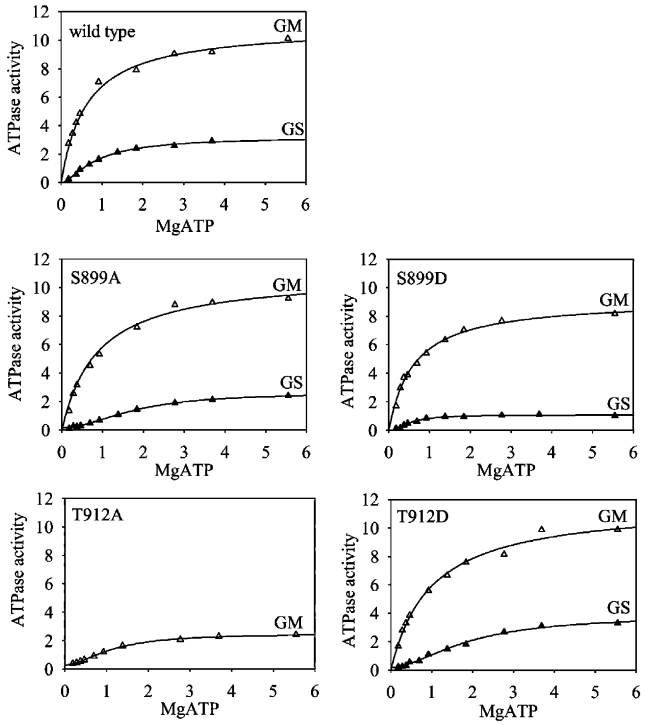

FIGURE 4: Effect of glucose activation on the kinetic properties of wild-type and mutant ATPases. Plasma membranes from GS and GM cells were assayed for ATPase activity over a range of MgATP concentrations from 0.2 to 6 mM. At each point, the specific activity was calculated as the difference between ATP hydrolysis in the absence and presence of 100 μM sodium orthovanadate. Data were fitted with either Michaelis−Menten (GM samples) or Hill (GS samples and T912A GM) equations using SigmaPlot software.

activation by glucose as described previously, with an increase in V_{max} [from 3.4 to 12.6 μmol/(mg·min)], increase in affinity for MgATP (evidenced as a lowering of the K_m from 1.9 to 0.7 mM), and decrease in IC_{50} for inorganic orthovanadate (from 5.3 to 0.8 μM). Also worth noting was the slight but reproducible cooperativity seen under carbon-starved conditions, with a Hill coefficient of 1.4.

Of the mutant ATPases, T912A was significantly altered in all of these properties. Plasma membranes from carbon-starved T912A lacked detectable H^+-ATPase activity, while the ATPase from glucose-metabolizing cells appeared kinetically similar to that seen in glucose-starved wild-type preparations, with a V_{max} of 2.5 μmol/(mg·min), K_m of 1.4 mM, IC_{50} of 3.5 μM, and Hill coefficient of 1.6. Thus, the T912A ATPase, although still sensitive to glucose metabolism, appears to be unable to attain the activated state. Only minor changes were seen in the other three mutants, which looked capable of full activation by glucose.

Effect of Ser-899 and Thr-912 Mutations on the Glucose-Dependent Conformational Change. When all four mutant ATPases were examined by limited trypsinolysis under GS and GM conditions, the two Ser-899 mutants displayed a normal glucose-dependent increase in trypsin sensitivity, while marked abnormalities were seen for the two Thr-912 mutants. In the experiment of Figure 5, wild-type and mutant plasma membranes were incubated with trypsin (1:4) for 15 min and analyzed by immunoblotting with anti-ATPase antiserum. Consistent with the kinetic data of Table 1, T912A ATPase showed clear signs of arrest in a trypsin-resistant conformation, even during glucose metabolism (GM condi-

Table 2: Effect of S899 and T912 Mutations on the Kinetic Properties of H^+-ATPase[a]

	V_{max} (units of P[b]/mg)			K_m(MgATP) (mM)		Hill coeff		IC_{50}(van) (μM)	
mutation	GS	GM	ratio	GS	GM	GS	GM	GS	GM
wild type	3.4	12.6	3.7	1.9	0.7	1.4		5.3	0.8
S899A	3.0	11.0	3.7	2.2	0.7	1.5		4.1	0.9
S899D	1.5	8.0	5.3	1.0	0.6	1.6		8.3	1.0
T912A	*c*	2.5	*c*	*c*	1.4	*c*	1.6	*c*	3.5
T912D	3.6	10.8	3.0	1.7	1.1	1.8		2.2	0.7

[a] Plasma membranes were isolated from glucose-starved (GS) or glucose-metabolizing (GM) cells. Vanadate-sensitive ATP hydrolysis was measured as described in Experimental Procedures. V_{max} and K_m were calculated by fitting the data with either the Michaelis−Menten equation (GM samples) or Hill equation (GS samples and T912A GM) using SigmaPlot W7. [b] One unit is defined as 1 μmol of P_i/min. Values are the mean of at least three determinations from different preparations, with a standard error less than 16%. [c] T912A ATPase had no detectable activity under GS conditions.

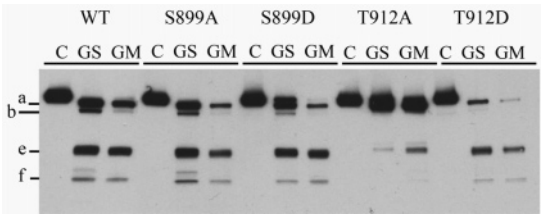

FIGURE 5: Trypsinolysis of S899A, S899D, T912A, and T912D ATPases. Plasma membranes from GS and GM cells were incubated at a trypsin:protein ratio of 1:4 for 15 min, and aliquots (0.5 μg of protein) were analyzed by immunoblotting with anti-Pma1 antiserum. C = control (undigested) membranes.

tions). By contrast, T912D ATPase was markedly sensitive to trypsin, even during glucose starvation (GS conditions).

In Figure 6, immunoblots of time-course digestions were scanned, and the combined intensity of the 100 and 98 kDa bands (which are difficult to resolve from one another) was plotted as a function of time. For the wild-type control, a significant difference in time course could be seen between the relatively resistant GS sample and the more sensitive GM sample. By contrast, there was little if any difference between the GS and GM samples of T912A ATPase, while T912D ATPase was sensitive under starvation conditions and even more so under glucose-metabolizing conditions. Thus, single point mutations at Thr-912 can have a profound influence on the glucose-dependent conformational change as tracked by limited trypsinolysis.

Further information came from limited trypsinolysis of the T912A ATPase in the presence and absence of MgADP and vanadate. In the immunoblot analysis of Figure 7, bands a, b, and e retained the ability to bind C-terminal antibody even under GM conditions, both in the presence and in the absence of ligands (panel B). Furthermore, in the absence of ligands or in the presence of vanadate, the 20 kDa carboxy-terminal fragment was now as prominent in GM samples as in GS samples (panel B). It is thus clear that the T912A mutation prevents the glucose-induced conformational change that exposes the C-terminal tail of the wild-type ATPase to trypsinolysis. However, the experiment of Figure 7 did give evidence for a more subtle glucose-dependent change in T912A: when the GM sample was treated with trypsin in the presence of vanadate, the characteristic v band appeared (panel A), pointing to a wild-type-like opening of the protein at or near Lys-174. The significance of these results will be discussed below.

DISCUSSION

Sites of Trypsinolysis in Wild-Type Pma1 ATPase. In this study, tryptic cleavage has served as a useful tool to probe the organization of cytoplasmic domains in yeast Pma1 H^+-ATPase. Trypsin begins by attacking the N-terminal part of the protein, cleaving first at Lys-28 (T1) and then at Arg-73 (T2) in the long segment leading up to transmembrane helix 1 (M1). This result agrees with earlier findings for the closely related Pma1 ATPase of *N. crassa* (*28*) and supports the idea of an extended conformation for the N-terminal segment, as modeled by Kuhlbrandt and co-workers (*13*; see below). A few minutes later, trypsin cleaves at Arg-271 (T3), near the junction between the A domain and M3 (Figure 1). Sensitivity to proteases in the A-to-M3 boundary region appears to be a general feature of P-type ATPases, since Na^+,K^+-, H^+,K^+-, and Ca^{2+}-ATPases are readily cut by trypsin, chymotrypsin, proteinase K, V8 protease, and/or papain at closely aligning sites (reviewed in ref *29*).

Three additional tryptic sites have been detected in yeast Pma1 ATPase, all of which are conformationally sensitive and capable of giving information about the reaction mechanism. Cleavage at T4 occurs in the unliganded protein and

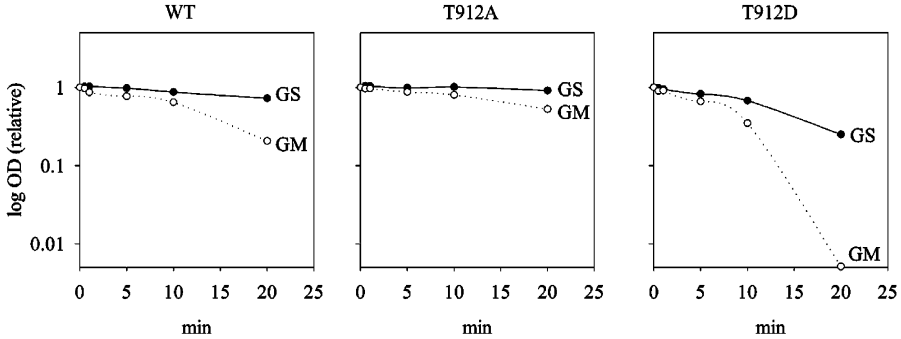

FIGURE 6: Effects of T912D and T912A mutations on the time course of trypsinolysis. Plasma membranes from GS and GM cells were incubated at a trypsin:protein ratio of 1:4 for 0−20 min, and aliquots (0.5 μg of protein) were immunoblotted with polyclonal anti-Pma1 antiserum. After scanning, the combined intensity of the 100 and 98 kDa bands was plotted as a function of digestion time.

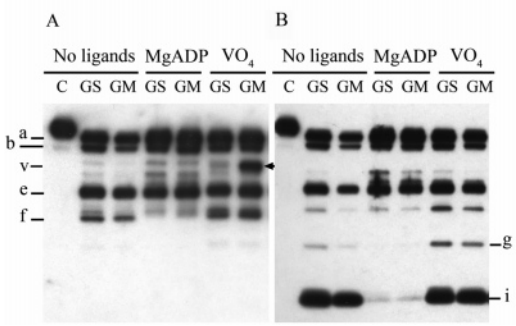

FIGURE 7: Effects of MgATP and vanadate on the trypsinolysis of T912A ATPase. This experiment was carried out as described in the legend to Figure 3.

in the presence of vanadate (E_2 state) but not in the presence of MgADP (E_1 state), giving rise to a 20 kDa band (i) that binds C-terminal antibody and is highly resistant to further proteolysis (Figure 3). On the basis of its apparent size, the 20 kDa band is likely to result from cleavage at Lys-749 or Lys-754 in the small cytoplasmic loop between M6 and M7. If so, it would correspond to the well-known carboxy-terminal 20 kDa fragment derived from Na^+/K^+-, H^+/K^+-, and SERCA Ca^{2+}-ATPases following extensive proteolytic digestion (*29*−*31*). In SERCA ATPase, the M6−M7 loop is similarly accessible to proteolysis in the presence of vanadate (E_2 state) but not in the presence of Ca^{2+} (E_1 state) (*31*). Consistent with this finding, recent crystal structures have shown that it is exposed at the surface of the protein in thapsigargin and vanadate-bound E_2 crystal structures of SERCA ATPase but becomes partially shielded in the Ca^{2+}-bound E_1 structure (*12*, *32*, *33*). Movement of the loop during the reaction cycle, along with its physical connection to M6 and M7, has led to the proposal that it may play a role in coupling between ATP hydrolysis and ion transport (*34*). The same may be true in yeast Pma1 ATPase where the M6−M7 loop, although shorter, is similar in amino acid sequence and conformational mobility.

T5 (Lys-174) lies near the cytoplasmic end of M2 and becomes accessible to trypsin in activated H^+-ATPase preparations from glucose-metabolizing cells. As in the case of T4, the cleavage product accumulates in the presence of vanadate (E_2 conformation) but not in the presence of MgADP (E_1 conformation). In SERCA Ca^{2+}-ATPase, a corresponding band results from protease K cleavage at Lys-120 and is prominent only in the absence of Ca^{2+} (E_2) (*29*). Recent studies have shown that proteolytic cleavage at this site (*35*) and site-directed mutations at nearby sites (Tyr-122 and Glu-123; *36*) lead to an important change in the reaction cycle of Ca^{2+}-ATPase, dramatically slowing the rate of dephosphorylation from E_2P to E_2. Indeed, the region defined by these residues has now been shown to lie at the interface between the A and P domains and to undergo a large conformational change during the E_1P to E_2P transition, when the A domain rotates, the N and P domains bend toward A to produce the "closed" E_2P structure, and M2 moves upward to bring its cytoplasmic end into close proximity with the P domain (*12*, *32*, *33*). The possible role of the homologous region in glucose activation of Pma1 H^+-ATPase will be discussed below.

Finally, the present study has provided clear evidence for one or more conformationally sensitive cleavage sites in the carboxy-terminal tail of Pma1 ATPase, since the tail is resistant to trypsinolysis in the carbon-starved state but is rapidly removed following activation by glucose. This region, too, will be discussed in greater detail below.

Figure 8 illustrates the positions of T1−T5 and the carboxy-terminal tail in a three-dimensional model of *Neurospora* Pma1 ATPase. In this model, built by Kuhlbrandt and co-workers (*13*), the *Neurospora* sequence was first aligned with that of SERCA Ca^{2+}-ATPase and mapped onto Toyoshima's 2.6 Å crystallographic structure of the SERCA enzyme (*12*, *37*). The result was then compared with an independently derived 8 Å structure of the *Neurospora* ATPase, obtained from two-dimensional crystals of the unliganded form of the enzyme (*38*). Models of the M and P domains proved to fit well within the 8 Å density map, and models of the N and A domains could also be accommodated by rigid-body displacement and rotation, respectively. The N- and C-terminal extensions could not be treated in the same way, given the lack of homology with

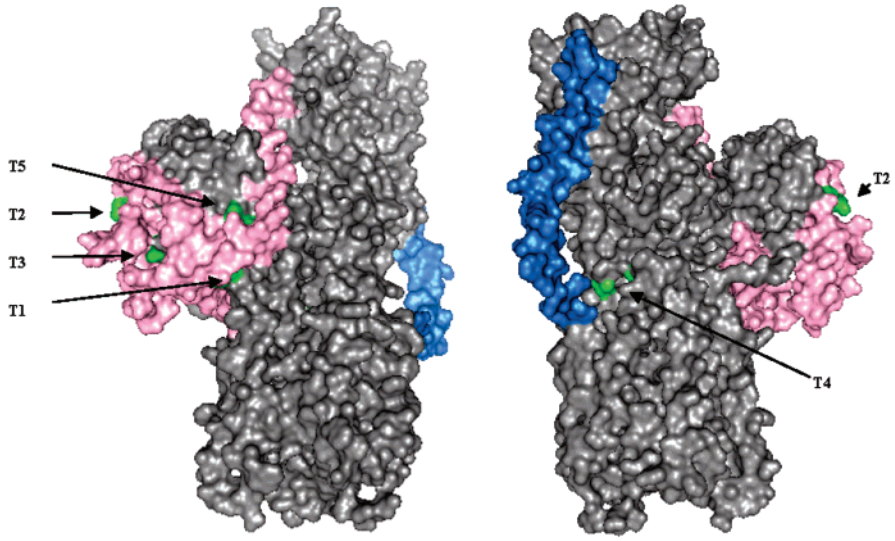

FIGURE 8: Three-dimensional model of the closely related Pma1 ATPase from *N. crassa* based on the analysis of Kuhlbrandt and co-workers (*13*). The extended N-terminal segment is highlighted in pink and the C-terminal segment in blue. Arrows indicate that tryptic sites T1−T5 (shown in green) are exposed at the surface of the ATPase.

SERCA ATPase, so they were simply placed within otherwise unoccupied regions of the 8 Å map. All five tryptic sites (T1−T5) identified in the present study lie partially or fully at the surface of the ATPase in the model, as does the carboxy-terminal tail.

Mechanism of Glucose Activation. A major goal of this study was to investigate the conformational change that takes place when yeast Pma1 ATPase is activated by growth on glucose. From limited trypsinolysis of the wild-type enzyme, it is clear that activation can be correlated with a general opening of the protein structure. Not only do GM samples display an overall increase in the rate of trypsinolysis compared with GS samples (Figure 1), but they show new sites of tryptic cleavage: within the C-terminal tail and, in the presence of vanadate, at the junction between M2 and the A domain (T5; Figure 2). Both of these sites shed useful light on the molecular mechanism of glucose activation. On the basis of the available crystal structures of SERCA Ca^{2+}-ATPase, Lys-174 lies at the junction between M2 and the A domain, close to the functionally important interface that forms between the A and P domains when E_2P is dephosphorylated to E_2 (*35*, *36*). In the case of the yeast H^+-ATPase, the accessibility of the T5 cleavage site only in GM samples points to a glucose-dependent conformational change in this region and raises the possibility that activation of the enzyme may reflect a change in the E_2P-to-E_2 part of the catalytic cycle.

The glucose-dependent opening of the carboxy-terminal tail to trypsinolysis is also worthy of mention. The tail is rich in Arg and Lys residues, which are hidden in the carbon-starved state but become accessible to trypsin under glucose-metabolizing conditions (Figure 3). This result provides direct support for the idea that the tail can act as an autoinhibitory domain, interacting tightly with the catalytic center of the ATPase during glucose starvation to downregulate enzymatic activity. Although there is little sequence homology among P-type ATPases in the carboxy-terminal region, similar conformational changes have been documented in PMCA Ca^{2+}-ATPase and plant plasma-membrane H^+-ATPases, where there is also good evidence for a regulatory role of the carboxyl terminus (*39*−*43*).

Key Role of Thr-912 in Glucose-Induced Unshielding of the C-Terminal Tail. With these results in mind, it was of interest to compare wild-type ATPase with mutants carrying amino acid substitutions at two consensus phosphorylation sites in the C-terminal regulatory domain, Ser-899 and Thr-912, residues already implicated in the kinetic changes seen upon glucose activation (*9*). While Ala and Asp substitutions at Ser-899 had little or no effect in the present study, mutations at Thr-912 led to significant changes in the response to glucose. In particular, T912A ATPase showed clear conformational characteristics of the glucose-starved state, with low sensitivity to trypsin even in GM samples, while T912D appeared at least partially locked in the glucose-metabolizing state, with marked trypsin sensitivity even in GS samples (Figure 6). Importantly, further probing with anti-C-terminal antiserum revealed that the carboxyl terminus, which normally becomes accessible to tryptic digestion in the GM state, remains shielded in T912A ATPase (Figure 7). Thus, kinase-mediated phosphorylation of Thr-912 may play a central role in freeing the carboxyl terminus from its autoinhibitory position. Consistent with this idea, measurements of ATP hydrolysis showed that T912A H^+-ATPase was unable to achieve a fully activated state during growth on glucose. Unlike GS samples, GM samples of the mutant ATPase displayed measurable activity, but all of the kinetic characteristics (K_m for MgATP, Hill coefficient, and IC_{50} for vanadate) remained similar to those of the glucose-starved state.

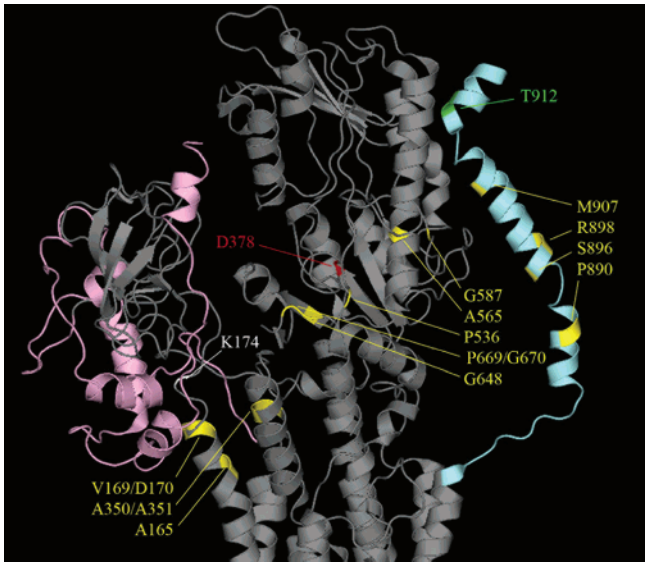

FIGURE 9: Three-dimensional model of the cytoplasmic domains of *Neurospora* Pma1 ATPase based on the analysis of Kuhlbrandt and co-workers (*13*). As in Figure 8, the N-terminal segment is highlighted in pink and the C-terminal segment in blue. Labeled in white is residue K174 (tryptic site T5, identified in this study and located at the boundary between the end of membrane segment 2 and the A domain), and labeled in green is T912 (putative site of kinase-mediated phosphorylation examined in this study). Highlighted in yellow are three groups of sites at which suppressors of the double mutant S911A/T912A have been mapped by Portillo and co-workers (*9*). See text for a discussion of the significance of the suppressors.

Directions for Future Research. Taken together, the results of this study have revealed structural and mechanistic similarities between Pma1 and mammalian P-type ATPases, including conformationally sensitive sites of proteolytic cleavage in boundary regions between the cytoplasmic and membrane domains. There are also clear differences, particularly with regard to the C-terminal tail. In Pma1, the tail is significantly longer than in Na^+,K^+- and SERCA Ca^{2+}-ATPases, and it changes in conformation to mediate glucose-dependent regulation of ATPase activity.

Still to be defined are the site or sites within the ATPase at which the C-terminal tail docks to exert its autoinhibitory action. In the model of Figure 9, which is based on cryoelectron microscopy of the *Neurospora* H^+-ATPase (*13*), most of the tail is depicted as relatively distant from the catalytic center of the protein. Recent genetic data raise the possibility of an alternative model, however, in which the tail may interact directly with the P and A domains of the ATPase. This idea is based on the work of Portillo and his group, in which intragenic suppressors were isolated starting with a double mutant (S911A/T912A) that exhibits little or no glucose activation and is unable to grow on glucose (*9*). Not surprisingly, four of the suppressors (P890opa, S896F, R898K, and M907I) map in the C-terminal region itself (Figure 9), but six of them (P536L, A565T, G587N, G648S,

P669L, and G670S) map in the P domain, in and around the aspartyl residue that is reversibly phosphorylated and dephosphorylated during the reaction cycle, and four (A165V, V169I/D170N, A350T, and A351T) cluster near the cytoplasmic ends of M2 and M4, between the A and P domains.

Bukrinsky and co-workers have pointed out that the latter two groups of suppressor mutations define a crude path from Ala-165 and Val-169/Asp-170 in the A domain to Ala-565 and Gly-587 in the P domain (see Figure 9) and have suggested that the carboxy-terminal tail may dock onto the Pma1 ATPase along that path (*44*). Interestingly, the tryptic cleavage site that is induced by vanadate in glucose-activated H^+-ATPase (Lys-174) lies close to the same path. More work is needed to determine the precise location of the carboxyl terminus and to define its movement between the inhibitory and activated states.

ACKNOWLEDGMENT

We thank Myron Crawford and Nancy Williams from Yale's W. M. Keck Foundation Biotechnology Resource Laboratory for expert assistance in peptide sequencing and members of the Slayman laboratory for helpful discussions.

REFERENCES

1. Morsomme, P., Slayman, C. W., and Goffeau, A. (2000) Mutagenic study of the structure, function and biogenesis of the yeast plasma membrane H^+-ATPase, *Biochim. Biophys. Acta 1469*, 133−157.
2. Kuhlbrandt, W. (2004) Biology, structure and mechanism of P-type ATPases, *Nat. Rev. Mol. Cell. Biol. 5*, 282−295.
3. Portillo, F. (2000) Regulation of plasma membrane H^+-ATPase in fungi and plants, *Biochim. Biophys. Acta 1469*, 31−42.
4. Serrano, R. (1983) In vivo glucose activation of the yeast plasma membrane ATPase, *FEBS Lett. 156*, 11−14.
5. Sychrova, H., and Kotyk, A. (1985) Conditions of activation of yeast plasma membrane ATPase, *FEBS Lett. 183*, 21−24.
6. Eraso, P., and Portillo, F. (1994) Molecular mechanism of regulation of yeast plasma membrane H^+-ATPase by glucose, *J. Biol. Chem. 269*, 10393−10399.
7. Venema, K., and Palmgren, M. G. (1995) Metabolic modulation of transport coupling ratio in yeast plasma membrane H^+-ATPase, *J. Biol. Chem. 270*, 19659−19667.
8. Portillo, F., Eraso, P., and Serrano, R. (1991) Analysis of the regulatory domain of yeast plasma membrane H^+-ATPase by directed mutagenesis and intragenic suppression, *FEBS Lett. 287*, 71−74.
9. Eraso, P., and Portillo, F. (1994) Molecular mechanism of regulation of yeast plasma membrane H^+-ATPase by glucose. Interaction between domains and identification of new regulatory sites, *J. Biol. Chem. 269*, 10393−10399.
10. Mason, A. B., Kardos, T. B., and Monk, B. C. (1998) Regulation and pH-dependent expression of a bilaterally truncated yeast plasma membrane H^+-ATPase, *Biochim. Biophys. Acta 1372*, 261−271.
11. Chang, A., and Slayman, C. W. (1991) Maturation of the yeast plasma membrane [H^+] ATPase involves phosphorylation during intracellular transport, *J. Cell Biol. 115*, 289−295.
12. Toyoshima, C., Nakasako, M., Nomura, H., and Ogawa, H. (2000) Crystal structure of the calcium pump of sarcoplasmic reticulum at 2.6 Å resolution, *Nature 405*, 647−655.
13. Kuhlbrandt, W., Zeelen, J., and Dietrich, J. (2002) Structure, mechanism, and regulation of the *Neurospora* plasma membrane H^+-ATPase, *Science 297*, 1692−1696.
14. Miranda, M., Allen, K. E., Pardo, J. P., and Slayman, C. W. (2001) Stalk segment 5 of the yeast plasma membrane H^+-ATPase: mutational evidence for a role in glucose regulation, *J. Biol. Chem. 276*, 22485−22490.
15. Miranda, M., Pardo, J. P., Allen, K. E., and Slayman, C. W. (2002) Stalk segment 5 of the yeast plasma membrane [H^+]-ATPase. Labeling with a fluorescent maleimide reveals a conformational change during glucose activation, *J. Biol. Chem. 277*, 40981−40988.
16. Sarkar, G., and Sommer, S. S. (1990) The "megaprimer" method of site-directed mutagenesis, *BioTechniques 8*, 404−407.
17. Nakamoto, R. K., Rao, R., and Slayman, C. W. (1991) Expression of the yeast plasma membrane [H^+] ATPase in secretory vesicles. A new strategy for directed mutagenesis, *J. Biol. Chem. 266*, 7940−7949.
18. Wang, G., Tamas, M., Pascual-Ahuir, A., and Perlin, D. S. (1989) Probing conserved regions of the cytoplasmic LOOP1 segment linking transmembrane segments 2 and 3 of the *Saccharomyces cerevisiae* plasma membrane H^+-ATPase, *J. Biol. Chem. 271*, 25438−25445.
19. Serrano, R. (1988) Structure and function of proton translocating ATPase in plasma membranes of plants and fungi, *Biochim. Biophys. Acta 947*, 1−28.
20. Perlin, D. S., Harris, S. L., Seto-Young, D., and Haber, J. E. (1989) Defective H^+-ATPase of hygromycin B-resistant pma1 mutants from *Saccharomyces cerevisiae*, *J. Biol. Chem. 264*, 21857−21864.
21. Lowry, O. H., Rosebrough, N. J., Farr, A. L., and Randall, R. J. (1951) Protein measurement with the Folin phenol reagent, *J. Biol. Chem. 193*, 265−275.
22. Ambesi, A., Allen, K. E., and Slayman, C. W. (1997) Isolation of transport-competent secretory vesicles from *Saccharomyces cerevisiae*, *Anal. Biochem. 251*, 127−129.
23. Fiske, C. H., and Subbarow, Y. (1925) The colorimetric determination of phosphorus, *J. Biol. Chem. 66*, 375−400.
24. Fabiato, A., and Fabiato, F. (1979) Calculator programs for computing the composition of the solutions containing multiple metals and ligands used for experiments in skinned muscle cells, *J. Physiol.* (*Paris*) *75*, 463−505.
25. Monk, B. C., Montesinos, C., Ferguson, C., Leonard, K., and Serrano, R. (1991) Immunological approaches to the transmembrane topology and conformational changes of the carboxyl-terminal regulatory domain of yeast plasma membrane H^+-ATPase, *J. Biol. Chem. 266*, 18097−18103.
26. Jorgensen, P. L., and Petersen, J. (1985) Chymotryptic cleavage of alpha-subunit in E1-forms of renal ($Na^+ + K^+$)-ATPase: effects on enzymatic properties, ligand binding and cation exchange, *Biochim. Biophys. Acta 821*, 319−333.
27. Blom, N., Gammeltoft, S., and Brunak, S. (1999) Sequence- and structure-based prediction of eukaryotic protein phosphorylation sites, *J. Mol. Biol. 294*, 1351−1362.
28. Mandala, S. M., and Slayman, C. W. (1989) The amino and carboxyl termini of the *Neurospora* plasma membrane H^+-ATPase are cytoplasmically located, *J. Biol. Chem. 264*, 16276−16281.
29. Sweadner, K. J., and Donnet, C. (2001) Structural similarities of Na,K-ATPase and SERCA, the Ca^{2+}-ATPase of the sarcoplasmic reticulum, *Biochem. J. 356*, 685−704.
30. Lutsenko, S., and Kaplan, J. H. (1994) Molecular events in close proximity to the membrane associated with the binding of ligands to the Na, K-ATPase, *J. Biol. Chem. 269*, 4555−4564.
31. Juul, B., Turc, H., Durand, M. L., Gomez de Gracia, A., Denoroy, L., Moller, J. V., Champeil, P., and le Maire, M. (1995) Do transmembrane segments in proteolyzed sarcoplasmic reticulum Ca^{2+}-ATPase retain their functional Ca^{2+} binding properties after removal of cytoplasmic fragments by proteinase K?, *J. Biol. Chem. 270*, 20123−20134.
32. Toyoshima, C., and Nomura, H. (2002) Structural changes in the calcium pump accompanying the dissociation of calcium, *Nature 418*, 605−611.
33. Toyoshima, C., and Mizutani, T. (2004) Crystal structure of the calcium pump with a bound ATP analogue, *Nature 430*, 529−535.
34. Lee, A. G., and East, J. M. (2001) What the structure of a calcium pump tells us about its mechanism, *Biochem. J. 356*, 665−683.
35. Lenoir, G., Picard, M., Gauron, C., Montigny, C., Le Marechal, P., Falson, P., Le Maire, M., Moller, J. V., and Champeil, P. (2004) Functional properties of sarcoplasmic reticulum Ca^{2+}-ATPase after proteolytic cleavage at Leu119-Lys120, close to the A-domain, *J. Biol. Chem. 279*, 9156−9166.
36. Yamasaki, K., Daiho, T., Danko, S., and Suzuki, H. (2004) Multiple and distinct effects of mutations of Tyr122, Glu123, Arg324, and Arg334 involved in interactions between the top part of second and fourth transmembrane helices in sarcoplasmic reticulum Ca^{2+}-ATPase: changes in cytoplasmic domain orga-

nization during isometric transition of phosphoenzyme intermediate and subsequent Ca^{2+} release, *J. Biol. Chem. 279*, 2202−2210.
37. Zhang, P., Toyoshima, C., Yonekura, K., Green, N. M., and Stokes, D. L. (1998) Structure of the calcium pump from sarcoplasmic reticulum at 8-Å resolution, *Nature 392*, 835−839.
38. Auer, M., Scarborough, G. A., and Kuhlbrandt, W. (1998) Three-dimensional map of the plasma membrane H^+-ATPase in the open conformation, *Nature 392*, 840−843.
39. Padanyi, R., Paszty, K., Penheiter, A. R., Filoteo, A. G., Penniston, J. T., and Enyedi, A. (2003) Intramolecular interactions of the regulatory region with the catalytic core in the plasma membrane calcium pump, *J. Biol. Chem. 278*, 35798−35804.
40. Palmgren, M. G., Sommarin, M., Serrano, R., and Larsson, C. (1991) Identification of an autoinhibitory domain in the C-terminal region of the plant plasma membrane H^+-ATPase, *J. Biol. Chem. 266*, 20470−20475.
41. Portillo, F. (2000) Regulation of plasma membrane H^+-ATPase in fungi and plants, *Biochim. Biophys. Acta 1469*, 31−42.
42. Morsomme, P., and Boutry, M. (2000) The plant plasma membrane H^+-ATPase: structure, function and regulation, *Biochim. Biophys. Acta 1465*, 1−16.
43. Palmgren, M. G. (2001) Plant plasma membrane H^+-ATPases: Powerhouses for nutrient uptake, *Annu. Rev. Plant Physiol. Plant Mol. Biol. 52*, 817−845.
44. Bukrinsky, J. T., Buch-Pedersen, M. J., Larsen, S., and Palmgren, M. G. (2001) A putative proton binding site of plasma membrane H^+-ATPase identified through homology modeling, *FEBS Lett. 494*, 6−10.

BI051555F